Extreme large mode area in single-mode pixelated Bragg fiber

Jean-Paul Yehouessi, Olivier Vanvincq, Andy Cassez, Marc Douay, Yves Quiquempois, Géraud Bouwmans, Laurent Bigot

Extreme large mode area in single-mode pixelated Bragg fiber

Jean-Paul Yehouessi,* Olivier Vanvincq, Andy Cassez, Marc Douay, Yves Quiquempois, Géraud Bouwmans, and Laurent Bigot

Univ. Lille, CNRS, UMR 8523 - PhLAM - Physique des Lasers Atomes et Molécules, IRCICA Institute 59658 Villeneuve d'Ascq, France

**Jean-Paul.Yehouessi@univ-lille1.fr*

Abstract: This paper reports the design and the fabrication of an all-solid photonic bandgap fiber with core diameter larger than 100 µm, a record effective mode area of about 3700 µm^2 at 1035 nm and robust single-mode behavior on propagation length as short as 90 cm. These properties are obtained by using a pixelated Bragg fiber geometry together with an heterostructuration of the cladding and the appropriated generalized half wave stack condition applied to the first three higher order modes. We detail the numerical study that permitted to select the most efficient cladding geometry and present the experimental results that validate our approach.

OCIS codes: (060.2280) Fiber design and fabrication; (060.2430) Fibers, single-mode; (060.5295) Photonic crystal fiber.

References and links

1. C. Jauregui, J. Limpert, and A. Tünnermann, "High-power fibre lasers," Nat. Photonics **7**(11), 861–867 (2013).
2. D. Jain, Y. Jung, P. Barua, S. Alam, and J. K. Sahu, "Demonstration of ultra-low NA rare-earth doped step index fiber for applications in high power fiber lasers," Opt. Express **23**(6), 7407–7415 (2015).
3. S. Lefrancois, C.-H. Liu, M. L. Stock, T. S. Sosnowski, A. Galvanauskas, and F. W. Wise, "High-energy similariton fiber laser using chirally coupled core fiber," Opt. Lett. **38**(1), 43–45 (2013).
4. L. Dong, T. W. Wu, H. A. McKay, L. Fu, J. Li, and H. G. Winful, "All-glass large-core leakage channel fibers," IEEE J. Sel. Top. Quantum Electron. **15**(1), 47–53 (2009).
5. J. Limpert, F. Stutzki, F. Jansen, H.-J. Otto, T. Eidam, C. Jauregui, and A. Tünnermann, "Yb-doped large-pitch fibres: effective single-mode operation based on higher-order mode delocalisation," Light Sci. Appl. **1**(4), e8 (2012).
6. R. Dauliat, D. Darwich, A. Benoît, R. Jamier, S. Grimm, K. Schuster, F. Salin, and P. Roy, "All-Solid Aperiodic Large Pitch Fibers for Operation in High Power Regime,"in *Proceedings of IEEE 17th International Conference on Transparent Optical Networks* (IEEE,2015), pp. 3–6.
7. X. Ao, T.-H. Her, and L. W. Casperson, "Gain guiding in large-core Bragg fibers," Opt. Express **17**(25), 22666–22672 (2009).
8. X. Peng, K. Kim, M. Mielke, T. Booth, J. W. Nicholson, J. M. Fini, X. Liu, A. Desantolo, P. S. Westbrook, R. S. Windeler, E. M. Monberg, F. V. Dimarcello, C. Headley, and D. J. Digiovanni, "Higher-order mode fiber enables high energy chirped-pulse amplification," Opt. Express **21**(26), 32411–32416 (2013).
9. D. A. Rockwell, V. V. Shkunov, and J. R. Marciante, "Semi-guiding high-aspect-ratio core (SHARC) fiber providing single-mode operation and an ultra-large core area in a compact coilable package," Opt. Express **19**(15), 14746–14762 (2011).
10. M. M. Jørgensen, S. R. Petersen, M. Laurila, J. Lægsgaard, and T. T. Alkeskjold, "Optimizing single mode robustness of the distributed modal filtering rod fiber amplifier," Opt. Express **20**(7), 7263–7273 (2012).
11. G. Gu, F. Kong, T. W. Hawkins, M. Jones, and L. Dong, "Extending mode areas of single-mode all-solid photonic bandgap fibers," Opt. Express **23**(7), 9147–9156 (2015).
12. D. Jain, Y. Jung, J. Kim, and J. K. Sahu, "Robust single-mode all-solid multi-trench fiber with large effective mode area," Opt. Lett. **39**(17), 5200–5203 (2014).
13. L. Dong, X. Peng, and J. Li, "Leakage channel optical fibers with large effective area," J. Opt. Soc. Am. B **24**(8), 1689–1697 (2007).
14. O. N. Egorova, S. L. Semjonov, A. F. Kosolapov, A. N. Denisov, A. D. Pryamikov, D. A. Gaponov, A. S. Biriukov, E. M. Dianov, M. Y. Salganskii, V. F. Khopin, M. V. Yashkov, A. N. Gurianov, and D. V. Kuksenkov, "Single-mode all-silica photonic bandgap fiber with 20-µm mode-field diameter," Opt. Express **16**(16), 11735–11740 (2008).

#255875 Received 17 Dec 2015; revised 7 Feb 2016; accepted 8 Feb 2016; published 25 Feb 2016

15. V. Pureur, L. Bigot, G. Bouwmans, Y. Quiquempois, M. Douay, and Y. Jaouen, "Ytterbium-doped solid core photonic bandgap fiber for laser operation around 980 nm," Appl. Phys. Lett. **92**(061113), 30–32 (2008).
16. O. N. Egorova, S. L. Semjonov, A. F. Kosolapov, V. V. Velmiskin, A. D. Pryamikov, A. S. Biriukov, M. Y. Salganskii, V. F. Khopin, M. V. Yashkov, A. N. Gurianov, and E. M. Dianov, "Large mode area single-mode ytterbium doped all-solid photonic bandgap fiber,"in *Proceedings of 35th Eur. Conf. Opt. Commun.* (2009), pp. 3–4.
17. D. A. Gaponov, P. Roy, S. Février, M. E. Likhachev, M. Y. Salganskii, and M. V. Yashkov, "100 W from a photonic bandgap Bragg fiber laser," Lasers Electro-Optics Quantum Electron. Laser Sci. Conf. (QELS), *2010 Conf.*, **vol. 2**, pp. 4–5, Optical Society of America 2010).
18. S. S. Aleshkina, M. E. Likhachev, A. D. Pryamikov, D. A. Gaponov, A. N. Denisov, M. M. Bubnov, M. Y. Salganskii, A. Y. Laptev, A. N. Guryanov, Y. A. Uspenskii, N. L. Popov, and S. Février, "Very-large-mode-area photonic bandgap Bragg fiber polarizing in a wide spectral range," Opt. Lett. **36**(18), 3566–3568 (2011).
19. M. Kashiwagi, K. Saitoh, K. Takenaga, S. Tanigawa, S. Matsuo, and M. Fujimaki, "Low bending loss and effectively single-mode all-solid photonic bandgap fiber with an effective area of 650 μm^2," Opt. Lett. **37**(8), 1292–1294 (2012).
20. X. Ma, C. Zhu, I.-N. Hu, A. Kaplan, and A. Galvanauskas, "Single-mode chirally-coupled-core fibers with larger than 50 μm diameter cores," Opt. Express **22**(8), 9206–9219 (2014).
21. A. Baz, L. Bigot, G. Bouwmans, and Y. Quiquempois, "Single-mode, large mode area, solid-core photonic bandgap fiber with hetero-structured cladding," J. Lightwave Technol. **31**(5), 830–835 (2013).
22. G. Gu, F. Kong, T. Hawkins, J. Parsons, M. Jones, C. Dunn, M. T. Kalichevsky-Dong, K. Saitoh, and L. Dong, "Ytterbium-doped large-mode-area all-solid photonic bandgap fiber lasers," Opt. Express **22**(11), 13962–13968 (2014).
23. B. Ward, "Solid-core photonic bandgap fibers for cladding-pumped Raman amplification," Opt. Express **19**(12), 11852–11866 (2011).
24. D. A. Gaponov, S. Février, M. Devautour, P. Roy, M. E. Likhachev, S. S. Aleshkina, M. Y. Salganskii, M. V. Yashkov, and A. N. Guryanov, "Management of the high-order mode content in large (40 μm) core photonic bandgap Bragg fiber laser," Opt. Lett. **35**(13), 2233–2235 (2010).
25. A. Baz, G. Bouwmans, L. Bigot, and Y. Quiquempois, "Pixelated high-index ring Bragg fibers," Opt. Express **20**(17), 18795–18802 (2012).
26. S. Ghosh, S. Dasgupta, R. K. Varshney, D. J. Richardson, and B. P. Pal, "Design of a Bragg fiber with large mode area for mid-infrared applications," Opt. Express **19**(22), 21295–21304 (2011).
27. J. P. Yehouessi, A. Baz, L. Bigot, G. Bouwmans, O. Vanvincq, M. Douay, and Y. Quiquempois, "Design and realization of flexible very large mode area pixelated Bragg fibers," Opt. Lett. **40**(3), 363–366 (2015).
28. O. Vanvincq, J. P. Yehouessi, G. Bouwmans, L. Bigot, and Y. Quiquempois, "Pixelated Bragg fibers : bandgap guiding, generalized half-wave stack condition, and application to large mode area fibers," J. Opt. Soc. Am. B **32**(9), 1986–1992 (2015).

1. Introduction

The large place occupied today by fiber laser systems on the laser marketplace is well explained by the advantages of this technology over other approaches based on bulk systems [1]. Beam quality, good thermal management and compactness are some of the intrinsic qualities of the fibers that are highly desired for industrial systems, for both generation and transport of intense laser light. So as to follow the demand of further increased beam power, Very Large Mode Area (VLMA) - i.e. fibers offering Mode Field Diameter (MFD) typically larger than 40 μm - and single-mode behavior are required. However, these contradictory properties are *a priori* impossible to obtain with conventional manufacturing process (i.e. core/cladding fibers made by CVD-based methods), the lowest Numerical Aperture (NA) reported up to now by such techniques being about 0.038 (i.e. core diameter of about 35 μm to obtain a single-mode behavior at 1 μm wavelength) [2]. This explains why an intense work has been focused on the study of various kinds of microstructured fiber geometries. This also opened up the way to different fibers geometries that are not intrinsically single-mode but whose core and/or cladding structure is designed so as to reject the undesired Higher Order Modes (HOM). This is the case for Chirally-Coupled-Core (CCC) fibers [3], Leaky-Channel Fibers (LCF) [4], Large-Pitch Fibers (LPF) [5], Fully-Aperiodic Large-Pitch-Fibers (FA-LPF) [6], gain-guiding fibers [7], HOM fibers [8], SHARC fiber [9], Distributed Mode Filtering fiber (DMF) [10], Solid-Core Photonic BandGap Fiber (SC-PBGF) [11] and Multi-trench fibers [12]. Figure 1 is an attempt to summarize the reports of record MFD at 1 μm wavelength as a function of years for two families of solid-core fibers, namely Modified-Total

#255875 Received 17 Dec 2015; revised 7 Feb 2016; accepted 8 Feb 2016; published 25 Feb 2016

Internal Reflexion (MTIR) guiding fibers and SC-PBGF, all reported as single-mode in practice by their authors.

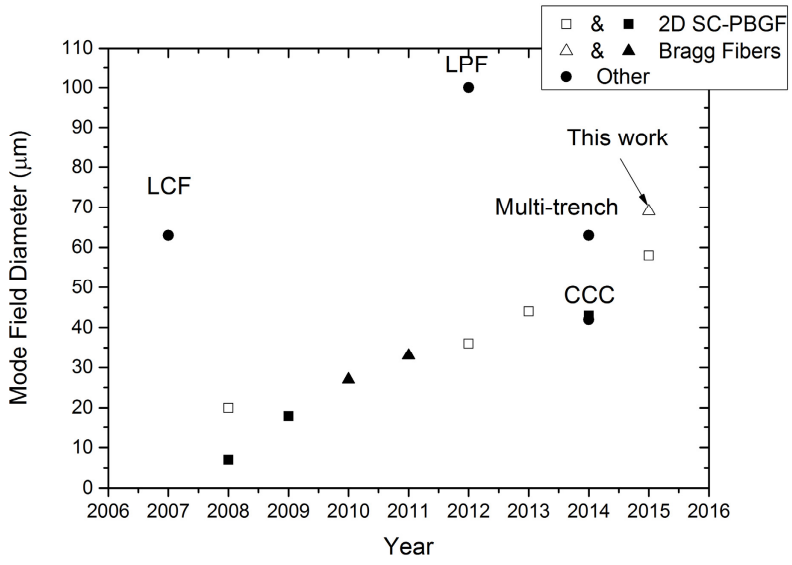

Fig. 1. Evolution of the mode field diameter of microstructured single mode fiber (dark symbols for doped fibers and white symbols for passive fibers). Results extracted from references [5,11–22].

Even if hardly comparable (some of these fibers being active, passive, polarization-maintaining or not), this figure demonstrates that only few solutions can propose MFD larger than 60 μm even in the case of passive fibers that are *a priori* more easy to realize. As mentionned above this figure also illustrates the growing performances of SC-PBGFs that today seem in position to compete with other fiber geometries while offering some added value like an all-solid structure that greatly facilitates fabrication and splicing or spectral filtering via photonic bandgap effect, which helps to reject undesired wavelengths (like, for example, the Raman effect [23]).

Among these fibers, 2D SC-PBGF [21] and Bragg fibers [24] are two possible options and, in the second case, the classical design has been recently revisited so as to improve the transmission properties of the fiber. More precisely, it has been proposed by our group to replace the high-index rings of classical Bragg fibers by discontinuous rings made of high index rods. This fiber design is known as Pixelated Bragg Fiber (PiBF) [25]. PiBF is good candidate for the realization of such single-mode fibers because the use of the appropriate Half Wave Stack (HWS) condition applied to low index ring helps to reject Higher Order Modes (HOM) and make the fiber single-mode [26]. Moreover, high-index rings were heterostructured by replacing some high-index rods by pure silica rods so as to enhance HOM leakage [27]. By combining these two different concepts, we have recently showed that pixelated Bragg fiber can be designed to obtain single-mode guidance and very low attenuation (below 25 dB/km between 1200 nm and 1500 nm) with core diameter as large as 48.5 μm [27].

The principal aim of this work is to extend the MFD of PiBF to more than 60 μm, such fiber entering into the category of Very Large Mode Area fibers (VLMA). Other aims are to simplify the PiBF manufacturing by reducing the number of high index rings from 3 to 2 and to take fully advantage of the filtering effect of the Photonic Bandgap (PBG) guidance by operating in a high order photonic bandgap window.

#255875 Received 17 Dec 2015; revised 7 Feb 2016; accepted 8 Feb 2016; published 25 Feb 2016

2. Numerical study

So as to reach a VLMA fiber design, two-rings PiBF with core diameter larger than 100 µm have been simulated. As in our previous work, the rings are composed of high index circular resonators with parabolic refractive index profile and a maximum refractive index difference of $30x10^{-3}$ as compared to silica (identical to that of a conventional multimode graded-index fiber). The resonators diameter, *d,* is 12 µm in order to work in the 5th bandgap at Yb operating wavelengths (900-1100 nm). The ratio between this diameter and the distance between two adjacent inclusions (Λ) is 0.53. This d/Λ value has been dictated mainly by manufacturing constraints: smaller values (as 0.36 in reference [27]) would lead to fewer resonators and thinner tubes for the low index ring while larger values (as 0.79 in reference [21]) would lead to a very large number of resonators to be stacked into a very small gap. Parametric study of the geometry of the heterostructuration of the two rings was done, starting from the study of a one-ring PiBF (diameter of the first high index ring about 116 µm, so this ring is composed of 16 rods) and then moving to a two-ring PiBF (diameter of second high index ring about 216.6 µm, so the second high-index ring is made of 30 rods) in order to insure robust single-mode behavior. Numerical results have been obtained through a vectorial Finite Element Method with anisotropic perfectly matched layer for confinement losses calculation

2.1 One-ring PiBF

Different symmetries of heterostructurations (without heterostructuration, π, π/2, quasi 2π/3, quasi 2π/5) are reported on Fig. 2 in the case of a PiBF comporting only one ring. The quasi 2π/5 heterostructuration symmetry presents the highest Confinement Losses (CL) for the Fundamental Mode (FM) and the lowest CL contrast between FM and HOM so this symmetry of heterostructuration will not be retained for the following. Non-heterostructured, π, π/2, quasi 2π/3 symmetries of heterostructuration show approximatively the same CL for FM (respectively 3 dB/m, 2.84 dB/m, 1.29 dB/m and 2.4 dB/m at 1030 nm). Non-heterostructured and π symmetry of heterostructuration present the two lowest CL for the first HOM (respectively 13.91 dB/m and 13.85 dB/m at 1030 nm) so they will not be chosen for the following. Situation is different for quasi 2π/3 and π/2 heterostructuration symmetries that present the lowest CL for FM and highest CL for the HOM so they are kept for the following.

It can be pointed out that without any heterostructuration of the ring [Fig. 2(a)] we note quite similar CL for all modes, together with a superposition of the curves for spatially degenerated modes. For π heterostructuration symmetry [Fig. 2(b)], different behaviors are observed for the spatially degenerated modes (namely $LP_{11a\&b}$ and $LP_{21a\&b}$), due to the fact that one modal orientation is less confined in the core than the other. It is, for example, the case for LP_{21a} that goes out from the core due to the field repartition of this mode that escapes through the voids made by the heterostructuration while the field distribution of mode LP_{21b} impede the leakage. For quasi 2π/3 heterostructuration symmetry [Fig. 2(c)] quasi equal CL are observed for the two spatial degeneracies of the LP_{11} modes and LP_{21} modes, respectively. π/2 heterostructuration symmetry [Fig. 2(d)] offers a larger difference of CL between the Fundamental Mode (FM) and first HOM, even if the LP_{21b} mode is still well confined due to the ring symmetry.

#255875 Received 17 Dec 2015; revised 7 Feb 2016; accepted 8 Feb 2016; published 25 Feb 2016

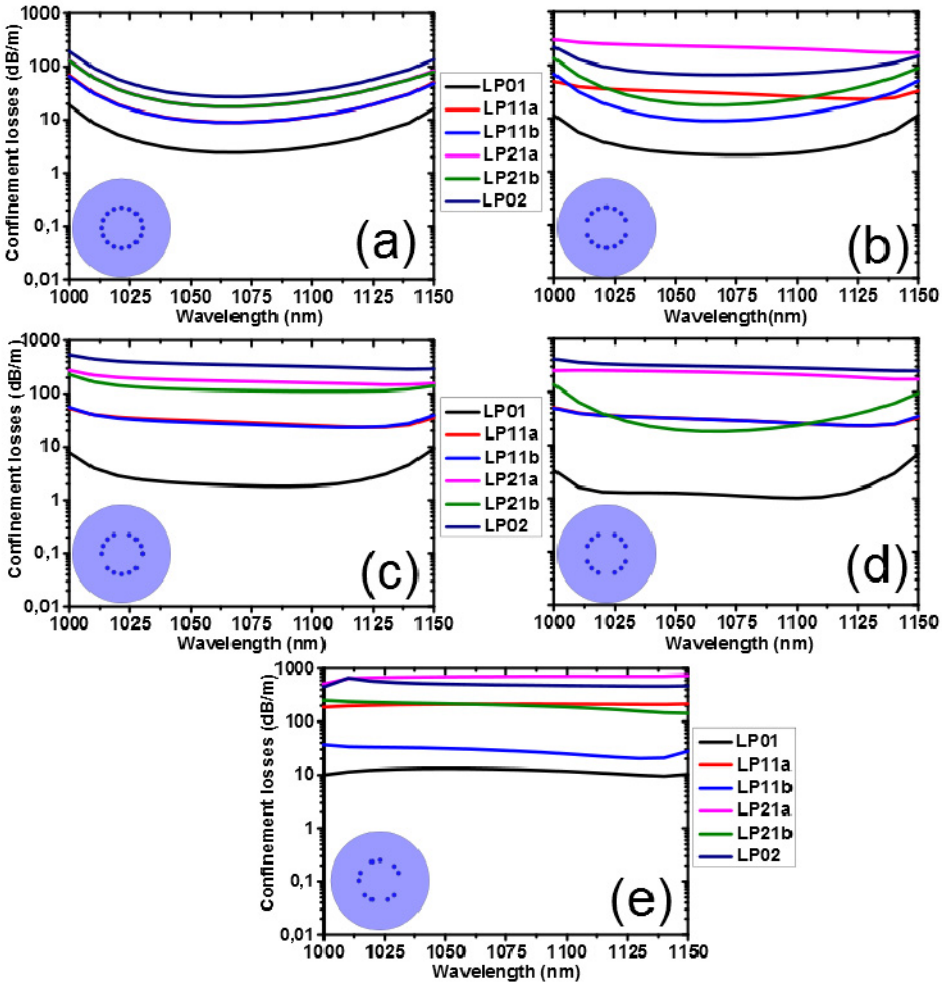

Fig. 2. Confinement losses for different geometries of pixelated Bragg fiber with only one index ring: (a) non-heterostructured, (b) π heterostructuration, (c) quasi 2π /3 heterostructuration, (d) π/2 heterostructuration, (e) quasi 2π/5 heterostructuration.

2.2 Two rings PiBF: heterostructuration of the first high index ring

The introduction of a second ring of high index resonators is necessary to reduce the CL of FM as well as to increase further the differential losses between FM and the HOMs by a judicious choice of the distance between the two high index rings. Indeed, this distance is chosen so as to permit the phase-matching condition between LP_{11}, LP_{21}, LP_{02} core modes with LP_{21}, LP_{51}, LP_{61} leaky modes of the low index ring (generalized half wave stack condition, see reference [28]). In the present case, this leads to a low index ring thickness of 38.3 µm. The benefit of this new structure can be clearly seen by comparing Fig. 2(c) and 2(d) with Fig. 3. Indeed, the CL of FM decrease by more than two orders of magnitude while the HOMs CL are reduced by only one order magnitude.

#255875 Received 17 Dec 2015; revised 7 Feb 2016; accepted 8 Feb 2016; published 25 Feb 2016

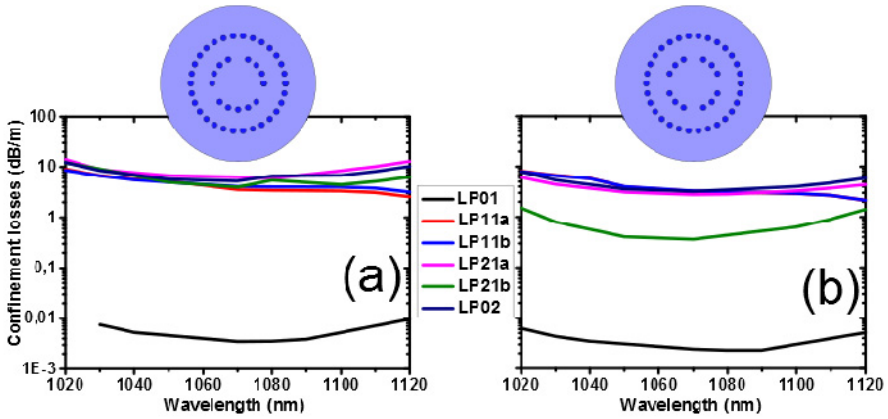

Fig. 3. Confinement losses for different geometries of pixelated Bragg fiber with two rings of high index inclusions for (a) quasi $2\pi/3$ symmetry of the first ring and (b) $\pi/2$ symmetry of the first ring.

The structure with quasi $2\pi/3$ heterostructuration symmetry is the most favorable: a difference of three orders of magnitude is observed between FM and first HOM CL [Fig. 3(a)] whereas only two orders of magnitude are predicted for the $\pi/2$ symmetry that is less adapted to reject the LP_{21b} mode [Fig. 3(b)]. The low confinement of HOM for the quasi $2\pi/3$ symmetry is illustrated in Fig. 4: the first ring heterostructuration permits couplings between core modes and low-index ring modes that are not allowed without heterostructuration due to symmetry consideration.

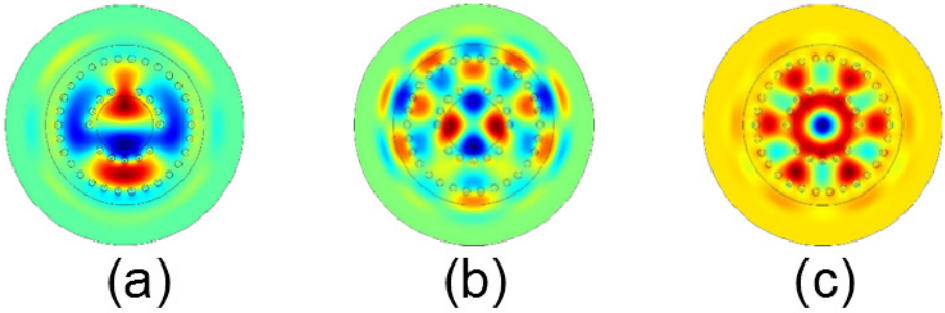

Fig. 4. Electric field distribution of LP_{11}(a), LP_{21}(b), LP_{02}(c) modes at 1050 nm for x-axis polarization. Strong couplings between LP_{11} core mode and LP_{21} claddding mode (a), LP_{21} core mode and LP_{51} cladding mode (b), LP_{02} core mode and LP_{61} cladding mode (c) are put in evidence.

#255875 Received 17 Dec 2015; revised 7 Feb 2016; accepted 8 Feb 2016; published 25 Feb 2016

2.3 Two rings PiBF: heterostructuration of the second high index ring

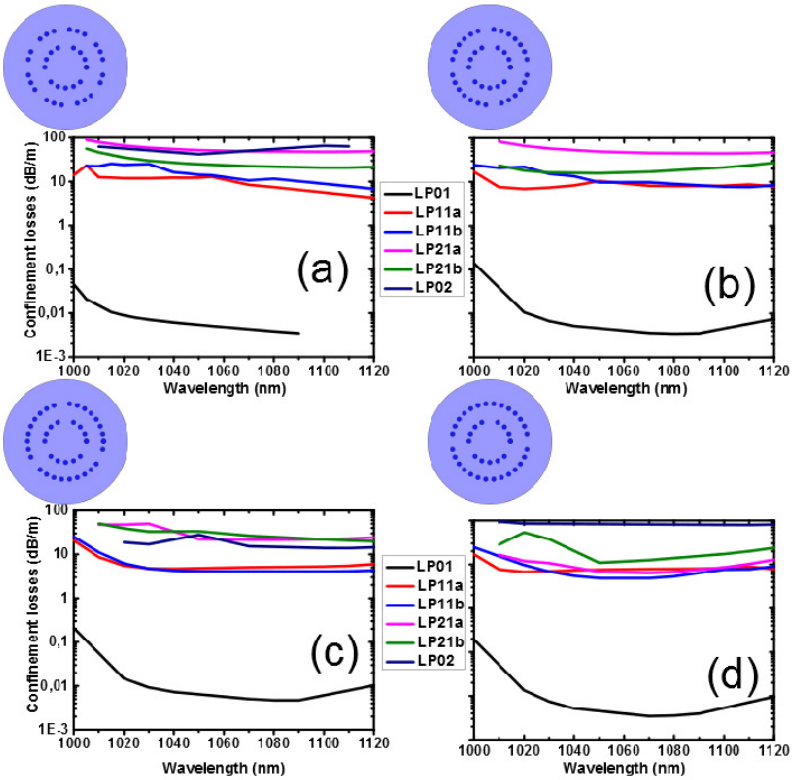

Fig. 5. Confinement losses for different geometries of pixelated Bragg fiber with quasi $2\pi/3$ heterostructuration symmetry for the first high index ring and for the second high index ring: (a) quasi $\pi/4$ heterostructuration, (b) quasi $\pi/2$ heterostructuration, (c) $2\pi/3$ heterostructuration, (d) π heterostructuration.

So as to improve even further the single-mode behavior, some high index resonators of the second ring were removed. On Fig. 5, the CL curves of four fibers with different symmetries of the second ring are reported for the quasi $2\pi/3$ symmetry selected in the previous section. It can be observed that the geometry of the second ring has a minor impact on CL of FM and a reduced effect on CL difference between FM and HOM, even if the number of voids is changed from 2 to 8. The CL of HOM are, however, maximized for the quasi $\pi/4$ symmetry [Fig. 5(a)] (As an example, at 1030 nm CL for LP_{11} are more than 12 dB/m and more than 30 dB/m for LP_{21} and LP_{02} modes) that will hence be chosen for the experimental realization.

3. Fabrication and experimental caracterisation

Based on the conclusions of the parametric approach detailed in the previous section, a fiber has been realized by the stack and draw technique. The core and the low index ring are made of pure silica elements (Suprasil F300, from Heraeus). High index inclusions are obtained from Germanium-doped preforms with parabolic index profile and core-to-cladding ratio of 0.53. The heterostructuration is obtained by replacing some high index inclusions with pure silica rods also made of Suprasil F300. The radius of the first and the second high index ring are respectively about 55.7 µm and 101.6 µm, those values are in good accordance with the theoretical design studied in the previous section (respectively 58 µm for the first index ring and 108.3 µm for the second high index ring). The analysis of SEM picture puts in evidence the deformation of the high index inclusions during the drawing process, these inclusions having a trapezoidal shape as shown in Fig. 6. The average measured dimension of high index

#255875 Received 17 Dec 2015; revised 7 Feb 2016; accepted 8 Feb 2016; published 25 Feb 2016

rod is 11.83 µm and center-to-center distance for two high index rods (pitch) is 21.5 µm, despite the deformation of the high index inclusions those values are also very closed to the simulated values (respectively 12 µm and 22.64 µm). Finally, the outside fiber diameter is very large (1.15 mm, like rod-type fibers) so that this fiber is not flexible.

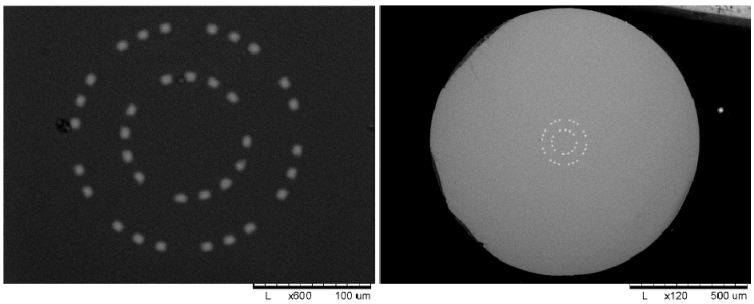

Fig. 6. SEM pictures for the fabricated fiber.

First the fiber transmission properties have been checked by injecting a supercontinuum source into a 90 cm-long piece of fiber maintained as straight as possible. The supercontinuum beam was injected via a HI1060 fiber, but-coupled to the PiBF and a second HI1060 was used to collect the output light into an optical spectrum analyser. Besides the above-mentionned deformation of the resonators, a photonic bandgap guidance is still possible and multiple transmission windows are observed, shown in Fig. 7. The wavelength of interest (λ = 1035 nm) is located in a transmission window limited to about 970 nm on the short wavenlength side and about 1070 nm on the long wavelength side. Due to the deformation of high index rods, couplings between core mode and high index inclusion modes are noticed inside each transmission window, as an example at 1010 nm, 1167 nm 1319 nm 1538 nm. An example of such couplings can be seen on Fig. 9 for the centered injection condition at 1010 nm. So these couplings reduce the previous transmission window of interest that now is limited to about 1010 nm on the short wavelength and 1070 nm on the long wavelength.

#255875 Received 17 Dec 2015; revised 7 Feb 2016; accepted 8 Feb 2016; published 25 Feb 2016

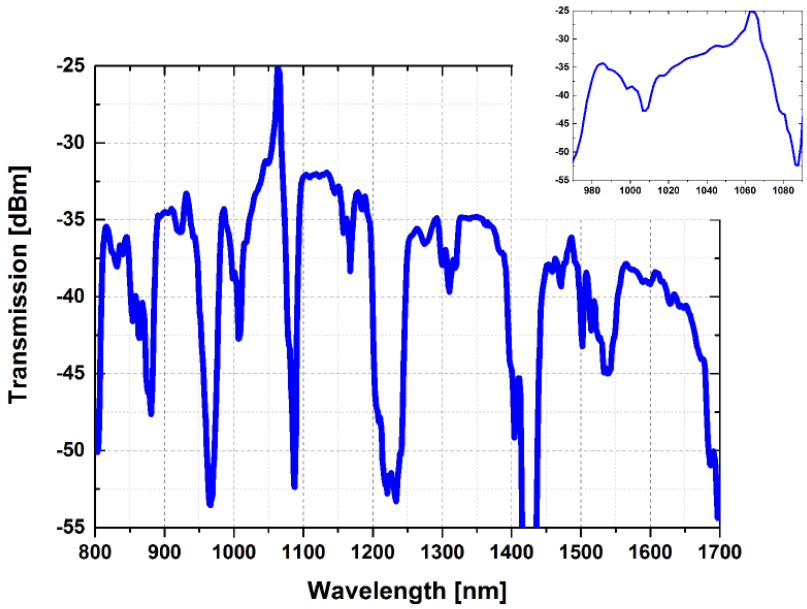

Fig. 7. Center: Transmission spectrum of a 90 cm-long piece of PiBF. Inset: Zoom-in figure of the transmission spectrum near 1035 nm.

The near field image was then studied in the same configuration (90 cm of straight fiber injected by coupling with a HI1060 fiber). Figure 8 shows the near-field image obtained at 1035 nm: the mode profile is very close to a Gaussian shape (for any cross section) with a MFD of 69 µm, corresponding to the largest MFD obtained in an all-solid photonic bandgap fiber shown in Fig. 1. Note that this high quality beam profile has been obtained despite the strong mismatch between the PiBF and HI1060 MFDs and the relatively short piece of straight fiber.

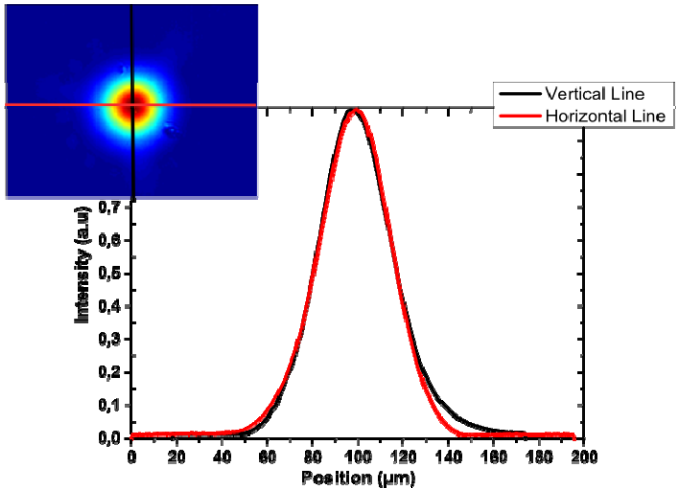

Fig. 8. Inset: Near field pattern of the core guided mode taken at 1035 nm for centered injection. Center: Beam profiles for vertical and horizontal cross-sections.

Single mode behavior is analyzed by off-centering the HI1060 fiber. An offset of respectively 20 µm and 36 µm is successively applied. Note that, in the last case, this value

#255875 Received 17 Dec 2015; revised 7 Feb 2016; accepted 8 Feb 2016; published 25 Feb 2016

represents more than 64% of the core radius (56 µm). So as to ensure that no bending effect can affect HOM propagation, fiber is kept as straight as possible. Near-field image are recorded by imaging the output facet on an InGaAs camera. Tested wavelengths have been chosen by using a narrow band filter inserted before the injection in the HI1060 fiber. No HOM can be identified for the different conditions of injection and for the different wavelengths even for a fiber shorter than one meter maintained as straight as possible see Fig. 9. The fiber can hence be considered as single-mode for this short length with stringent testing conditions for wavelength between 1010 nm and 1035 nm. If required, this spectral window may be increased by reducing the deformations of the high index inclusions during the fabrication.

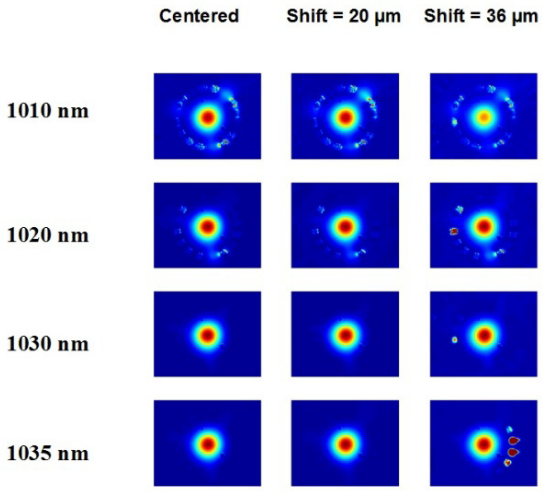

Fig. 9. Near field pattern of the core guided mode taken with narrow-band filters for a 90 cm-long straight fiber. From left to right: images obtained for centered injection, off-set of 20 µm and off-set of 36 µm. Each line corresponds to a wavelength.

Conclusion

It is shown that pixelated Bragg fiber geometry can be simplified to obtain a single-mode behavior with a cladding composed of only two rings of high index inclusions. Combining this simplified approach to an adapted symmetry of heterostructuration of the rings, single mode behavior has been observed even for a fiber shorter than one meter. This behavior is observed for a transmission bandwidth of several tens of nanometers. At 1035 nm wavelength, a MFD value of 69 µm is recorded, which represents a record in the case of all solid photonic bandgap fibers. We believe that this design represents excellent basis for the realization of VLMA fibers.

Acknowledgments

This work is partly supported by the French Ministry of Higher Education and Research, the Nord Pas-de-Calais Regional Council and “Fonds Européen de Développement Économique Régional” through the Labex CEMPI (ANR-11-LABX-0007) and Equipex FLUX (ANR-11-EQPX-0017). We thank Remi Habert for technical assistance.

#255875 Received 17 Dec 2015; revised 7 Feb 2016; accepted 8 Feb 2016; published 25 Feb 2016